On-line measurement of battery impedance using motor controller excitation

David A. Howey *Member, IEEE*, Paul D. Mitcheson *Member, IEEE*,
Vladimir Yufit, Gregory J. Offer, Nigel P. Brandon

***Abstract*—This paper presents a fast, cost effective technique for the measurement of battery impedance on-line in an application such as an electric or hybrid vehicle. Impedance measurements on lithium-ion batteries between 1 Hz and 2 kHz give information about the electrochemical reactions within a cell, which relates to state of charge, internal temperature and state of health. We concentrate on the development of a measurement system for impedance that for the first time uses an excitation current generated by a motor controller. Using simple electronics to amplify and filter the voltage and current, we demonstrate accurate impedance measurements obtained with both multi-sine and noise excitation signals, achieving RMS magnitude measurement uncertainties between 1.9% and 5.8% in comparison to a high accuracy laboratory impedance analyser. Achieving this requires calibration of the measurement circuits, including measurement of the inductance of the current sense resistor. A statistical correlation approach is used to extract the impedance information from the measured voltage and current signals in the presence of noise, allowing a wide range of excitation signals to be used. Finally, we also discuss the implementation challenges of a state of charge estimation system based on impedance.**

***Index Terms*—Impedance spectroscopy, battery, electric vehicle, hybrid vehicle, condition monitoring, state of charge**

I. Introduction

Electric and hybrid vehicles employ a battery management system (BMS) to monitor and control battery voltages, currents and temperatures for safety reasons, and to calculate battery state of charge (SOC), state of health (SOH) and other performance metrics. With respect to SOC, the most basic systems measure only steady state values and use coulomb counting, with an empirical model and lookup table of previously measured characteristic parameters to account for changes in performance at different charge and discharge rates and with age [1]. More sophisticated systems use adaptive state estimation to fit parameters on-line, e.g. [2], [3].

Electrochemical impedance spectroscopy (EIS) is a powerful tool to investigate the fundamental electrochemical reactions occurring within cells. EIS measurements are obtained by varying the voltage and current of a cell at different frequencies in order to measure the impedance of the cell as a function of frequency. With accurate calibration and in combination with other methods, this technique can be used to gain vital information about SOC and SOH of batteries, e.g. [4]. Impedance measurement may also be used to detect and analyse faults in battery packs [5]. However, although EIS has been widely applied in the laboratory, it is a relatively specialised technique normally requiring expensive and bulky equipment to achieve accurate results [6]. There is growing interest in the use of EIS for 'in situ' condition monitoring of batteries for a variety of applications. In this paper, our main goal is to demonstrate a low cost but accurate excitation and measurement system for impedance that could be used online in a vehicle or other application.

The overall system schematic of this work is illustrated in Fig. 1 in relation to an electric vehicle drive system. An impedance measurement system comprises an excitation system to perturb the cells, and a measurement and signal processing system to calculate the impedance. In our system, the excitation in current comes either from variations in the main traction current due to driver response, controller response, from an optional additional excitation circuit not discussed here, or a combination of all of these. In this paper we control both an electronic load and a motor controller to investigate these techniques. The electronic load was included since it allows a responsive and relatively low noise control of battery current. This enabled the development and verification of our hardware and signal processing approaches before moving to the much more challenging environment presented by a motor controller. The measurement and processing system consists of voltage and current measurement plus amplification and filtering, then digital processing to determine the cell's impedance as a function of frequency. Our focus here is to demonstrate a low-cost excitation and measurement system, and therefore we only briefly explore the implementation challenges of an impedance-based SOC estimation system as a first example of what could be inferred from impedance (see section VI). In relation to this, Fig. 2 shows the measured variation in impedance with SOC for a lithium-ion iron phosphate (LFP) A123 Systems cell (ANR26650M1A, 2.3 Ah), obtained using a Bio-Logic VSP multichannel potentiostat and frequency response analyser in galvanostatic mode with $\pm$250 mA peak current fluctuations and zero DC current. As can be seen, impedance varies with SOC and could therefore be used for

D.A. Howey is based at the Department of Engineering Science, University of Oxford, UK, email david.howey@eng.ox.ac.uk.

P.D. Mitcheson is based at the Department of Electrical and Electronic Engineering, Imperial College, Exhibition Road, London, SW7 2AZ, UK.

V. Yufit and N.P. Brandon are based at the Department of Earth Science and Engineering, Imperial College London.

G.J. Offer is based at the Department of Mechanical Engineering, Imperial College London.

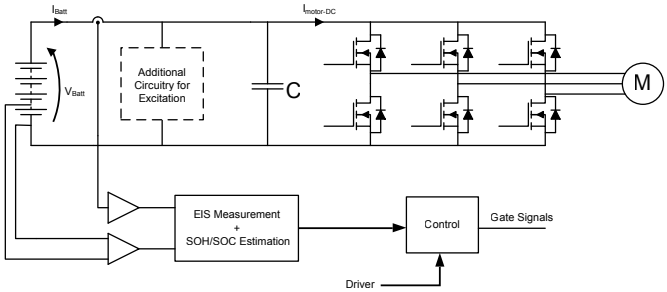

Fig. 1. Battery impedance measurement within vehicle drivetrain

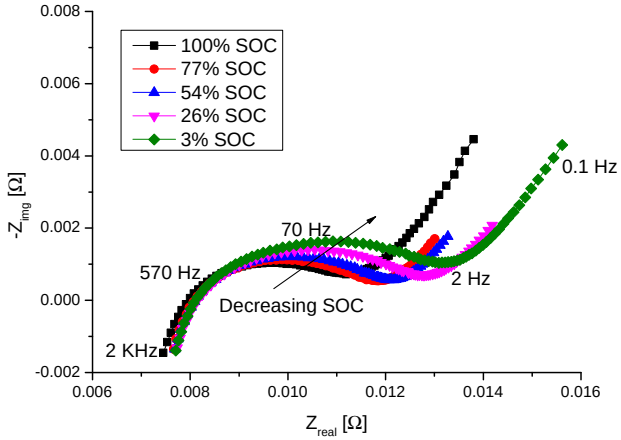

Fig. 2. Variation in LFP cell impedance with SOC (x-axis shows real part of impedance, y-axis shows negative reactive part)

direct SOC estimation. Cell temperature, SOH and DC offset current also affect the impedance and must be accounted for when using impedance to determine SOC.

Impedance spectroscopy is a useful tool for indirectly inferring SOC, but there is a noted lack of available equipment for on-vehicle impedance measurement [2]. Impedance spectra for lead acid cells in stationary applications have been measured using naturally present system noise as the excitation [7], but this required a commercial laboratory impedance analyser.

Bespoke current perturbation and impedance measurement circuitry for lead acid cells was developed by Fairweather et al. who demonstrated the use of pseudo random binary sequences (PRBS) as an excitation signal. The SOC and cold cranking (pulse discharge) capability of lead acid cells has been shown to relate directly to impedance and Blanke, Bohlen et al. [8], [9] developed bespoke circuitry for the prediction of cold cranking capability using electrical noise present on the vehicle power bus.

The use of actively applied broadband noise to measure lithium-ion battery impedance by cross-correlation of the voltage and current measurements was investigated by Christopherson et al. [10]. However, the results required extensive spectral averaging taking a number of minutes, and were inconclusive as they exhibited some significant phase measurement error which highlights the difficulty in obtaining accurate results. The authors have since pursued an alternative approach using multi-sine excitation with compensated synchronous detection and have several patents in this area (e.g. [11]).

Considerable research has also focused on describing and modelling the impedance response of lithium ion batteries under various conditions, which is necessary to develop an impedance-based BMS. Of relevance are papers by Doyle et al. [12] who developed a mathematical model to simulate lithium battery impedance, and Barsoukov et al. [13] who describe an impedance parameterization procedure. Troltzsch et al. [4] showed that series resistance, charge transfer resistance and Warburg coefficient change significantly during battery ageing. The use of voltage and current pulses occurring during normal vehicle operation to estimate internal resistance as a marker of battery ageing was demonstrated by Remmlinger et al. [14]. Roscher el al. [15] also show that the battery impedance increases with ageing during high current pulses.

This brief review of the literature shows that there are relatively few examples of EIS being applied outside the laboratory and there is scope for development of this technique for direct online condition monitoring. However, a low cost, simple, lightweight but sufficiently accurate system is required.

There are significant challenges to overcome for the accurate measurement of battery impedance in automotive applications because the batteries exhibit extremely low impedance values (of the order of mΩ) and therefore the small signal perturbation in voltage response is of the order of mV or less (see Fig. 6). In addition the phase of the battery impedance is typically small, between -10 and +10 degrees. Associated issues are: (a) achieving a good signal-to-noise ratio without causing the battery to behave non-linearly, (b) ensuring a sufficiently fast measurement so that time invariance can be assumed and, (c) accurate measurement of absolute magnitude and phase of voltage and current. These challenges are explored in the remainder of this paper, in section II with respect to issues (a) and (b), and section III with respect to issue (c).

II. Impedance Estimation Techniques

A. Overview

Impedance measurement may be considered to be a form of system identification. With a sufficiently small current and voltage perturbation the response of an electrochemical cell may be assumed to be linear. The small signal current fluctuation $i(t)$ is the system input and the resulting small signal voltage fluctuation $v(t)$ is the output, with the impedance being the system transfer function relating current to voltage:

$$V(s) = Z(s)\, I(s) \tag{1}$$

where $V(s)$ is the frequency domain voltage signal, $I(s)$ the frequency domain current signal and $Z(s)$ the frequency domain impedance. This is illustrated in Fig. 3 which also shows the addition of unknown uncorrelated output noise $n(t)$ which is unavoidably measured together with the voltage

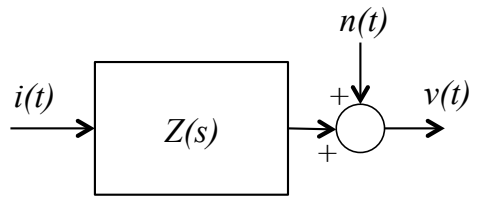

Fig. 3. Impedance represented as a transfer function

response. For accurate measurement the impact of this noise must be estimated. In practice the signals are usually discrete time sampled, however in this paper we present the analysis in continuous time.

A suitable excitation signal must be chosen and signal processing algorithms are then used to extract the wanted impedance from the measurements in the presence of unwanted noise. A wide variety of common approaches are possible. We give a short overview of the four main approaches below in order to motivate and set in context our chosen approach described in section II-E.

B. Single sine frequency sweep with phase detector

This is the most common approach used in electrochemical laboratories, with good noise rejection. However, it is relatively slow and this can lead to non steady state cell behaviour during measurement. A persistent single frequency sinusoidal current excitation $i(t)$ is applied and the voltage response $v(t)$ measured; this is then repeated at each frequency of interest:

$$i(t) = Icos\,(\omega t) \tag{2}$$

$$v(t) = Vcos\,(\omega t + \phi) \tag{3}$$

where I is the RMS current, V is the RMS voltage and ϕ is the phase difference between current and voltage. The impedance magnitude at the frequency ω is given by the ratio V/I and the phase ϕ is calculated with a phase detector, which mixes the current with direct and quadrature voltage measurements then low pass filters the results to leave DC components proportional to the sine and cosine of ϕ. In order to generate the high quality pure sinusoid excitation signal required to implement this approach, a direct digital synthesis (DDS) chip can be used. Integrated solutions such as Analog Devices AD5933 provide the DDS together with digital-to-analog and analog-to-digital converters and suitable processing.

C. Multisine excitation with Fourier transforms

A number N of persistent concurrent multiple sinusoids at frequencies ω_k may be applied as an excitation:

$$i(t) = \sum_{k=1}^{N} sin\,\omega_k t \tag{4}$$

A windowed Fourier transform of the measured voltage and current can be used to calculate the impedance, i.e.:

$$\hat{Z}(\omega) = \frac{V(\omega)}{I(\omega)} \tag{5}$$

where $V(\omega)$ is the Fourier transform of the voltage response and $I(\omega)$ is the Fourier transform of the current excitation signal. The estimated impedance $\hat{Z}(\omega)$ is only valid at frequencies where $I(\omega) \neq 0$. A multisine excitation signal can be synthesised using a digital signal processor (DSP) and digital-to-analog converter. A key consideration is that all frequencies ω_k should be integer multiples of the lowest frequency to ensure periodicity. Also, the phases of the synthesised components must be randomised to normalise the total signal amplitude.

D. Time domain step response with Fourier transforms

The estimated impedance in response to an impulse magnitude α is given by (Ljung [16]):

$$\hat{Z(t)} = \frac{v(t)}{\alpha} \tag{6}$$

The estimate $\hat{Z}$ in response to a step input is similar but with the derivative of $v(t)$ as the numerator.

Impulse and step responses have the significant disadvantage that due to the small impedances typical of batteries, the measured response $v(t)$ is of small amplitude in comparison to the noise $n(t)$ and therefore very large inputs are required for good signal-to-noise ratio, which results in non-linear behaviour [16]. Further noise is introduced by differentiating $v(t)$ for the step input case. Therefore these approaches are not pursued further in this paper.

E. Broadband excitation with stochastic approaches

This section describes our chosen method of signal processing. The frequency response of a system to a non-deterministic input signal may be computed by dividing the cross spectral density $S_{iv}(\omega)$ between input and output signals by the input power spectral density $S_{ii}(\omega)$ i.e.:

$$\hat{Z}(\omega) = \frac{S_{iv}(\omega)}{S_{ii}(\omega)} \tag{7}$$

where according to the Wiener-Khintchine theorem the power spectral density of a wide sense stationary signal is given by the Fourier transform of the autocorrelation function r_{ii}:

$$S_{ii} = \int_{-\infty}^{\infty} r_{ii}(\tau) e^{-j\omega\tau} d\tau \tag{8}$$

Similarly the cross spectral density is given by the Fourier transform of the cross-correlation function r_{iv}:

$$S_{iv} = \int_{-\infty}^{\infty} r_{iv}(\tau) e^{-j\omega\tau} d\tau \tag{9}$$

where the cross-correlation (assuming ergodicity) is:

$$r_{iv}(\tau) = \lim_{T\to\infty} \int_{-T}^{+T} i(t)v(t+\tau)dt \tag{10}$$

This approach is usually used with band-limited white noise as an excitation input signal. This may be generated using a random or pseudo-random number sequence which may be pre-stored in a look up table.

Similarly, pseudo-random binary sequences (PRBS) are repeating binary sequences that may also be used as excitation signals, since in the frequency domain they approximate band-limited white noise [17]. A PRBS may be pre-generated in software and stored in a lookup table. Both the bandwidth and the frequency resolution may be adjusted by adjusting the clock frequency and number of stages in the PRBS generator. Full details may be found in [18].

In order to smooth a frequency response estimate measured with noise excitation, spectral averaging is used, i.e. convolution of $\hat{Z}(\omega)$ with a window function such as a Hamming or Bartlett window. This reduces the estimate variance at the expense of introducing bias to the estimate. In our system, spectral averaging with a rolling average of 10 data blocks was sufficient to obtain good quality impedance data. Additionally, it is useful to truncate the estimated frequency response above some frequency, in our system this frequency was 2 kHz.

The advantage of using a correlation-based approach is that a wide range of excitation signals may be used. However, one must distinguish between the desirable signal caused by the impedance and undesirable interference S_{nn}, added to the measurement at the system output (see Fig. 3):

$$S_{vv} = |Z(\omega)|^2 S_{ii} + S_{nn} \tag{11}$$

It is impossible to measure the magnitude of S_{nn} directly, but its impact may be estimated using the quadratic coherence spectrum, which returns a value between zero and one:

$$\gamma^2(\omega) = \frac{|S_{iv}(\omega)|^2}{S_{ii}(\omega)S_{vv}(\omega)} \tag{12}$$

The coherence spectrum γ^2 is a frequency dependent correlation coefficient between two signals, useful both as a test of linearity and signal-to-noise ratio. If $\gamma^2 = 0$ then $i(t)$ and $v(t)$ are unrelated, and if $\gamma^2 = 1$ then they are completely related by a linear transfer function. In practice, at each frequency, $0 < \gamma^2 < 1$ due to the presence of undesired measurement noise, nonlinearity, or inputs which have not been measured. The coherence function therefore gives a very useful method to remove poor quality frequency response data. This may be achieved by ignoring data at frequencies where $\gamma^2 < t_h$ where t_h is a suitable coherence threshold, for example $t_h = 0.9$.

Due to its flexibility and ability to reject interference, we selected the method described in this section for implementation. Our chosen approach for estimation of impedance is to use equation 7 to obtain $\hat{Z(\omega)}$ from time domain measured voltage and current data, provided that $\gamma^2(\omega) > t_h$ for each value of ω. This was implemented in LabVIEW using standard library functions.

III. Experimental system

In this section we discuss the design and calibration of suitable measurement hardware to obtain the voltage and current measurements that may be used to estimate $\hat{Z(\omega)}$ with the technique as explained in the previous section.

A. Hardware design

Two methods were used to excite the battery current: an electronic load (TTi LD300) with external control signal, and a motor controller (Elmo Piccolo) plus brushless permanent magnet motor (Maxon EC 45) in current control mode. The approach using the motor drive is intended to demonstrate how this system might work in a vehicle application, see Sec. V. A National Instruments data acquisition system (NI 6211) was used for analog and digital input and output, controlled by a computer.

Fig. 4 shows the impedance measurement system built around the electronic load with current and voltage measurement. The measurement circuits consist each of a unity gain differential instrumentation amplifier A1 (Analog Devices AD627) followed by a passive RC high pass filter plus non-inverting op-amp gain stage A2 (Analog Devices OP97) configured for a gain of 100. The passive filter was chosen to have a low frequency -3dB point around 1 Hz by selecting $C \approx 12\ \mu$F and $R \approx 10\ k\Omega$, at which the phase shift is $+45°$. The expected roll-off at low frequency is 20 dB per decade as this is a first order filter. The reason for choosing this cut-off frequency was because we are interested in capturing impedance at relatively higher frequencies (around 10-2000 Hz for example) in order to make a fast measurement that does not interfere with other aspects of the end-use application and to avoid non-stationary battery behaviour. These frequencies are sufficient to capture electric double layer, charge transfer, solid-electrolyte interphase (SEI) transport, inductance and series resistance effects in a battery, as well as some mass transport diffusion effects [19]. Accurate measurement of double layer capacitance, charge transfer resistance and series resistance, all of which are possible at these frequencies, may be used to indicate SOC, SOH and temperature [20]. The current measurement circuit used a precision shunt resistor R_s combined with similar amplifiers as used on the voltage measurement circuit.

Both A1 and A2 have non-zero input offset voltages. The high pass filter stage ensures that any DC offset from A1 is removed; any DC offset from A2 is removed in software.

B. Calibration of measurement channels

The frequency response of each measurement channels will affect the measured results but this can be compensated for as described in this section in order to achieve an accurate absolute measurement with low cost equipment. Such an approach is preferable to using an expensive, complex set of filters to achieve a flat frequency response. It was assumed

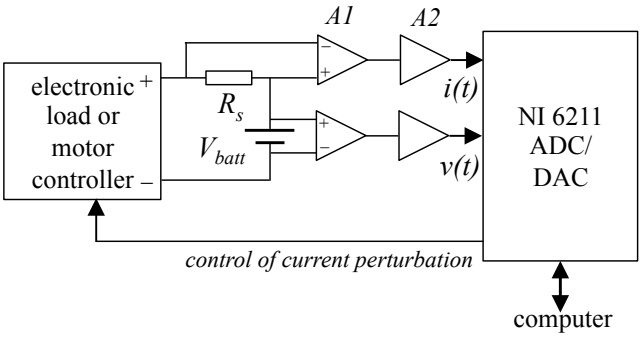

Fig. 4. Impedance measurement system for a single cell

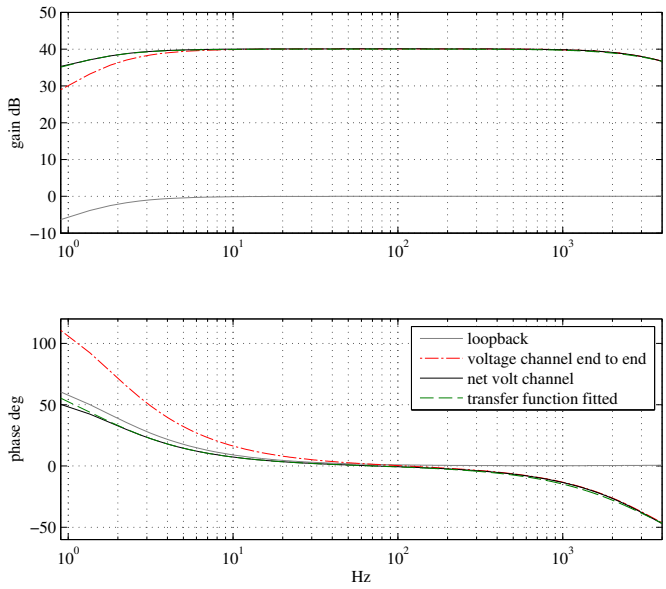

Fig. 5. Voltage channel measured response using network analyser

throughout that all elements behave linearly. Calibration of the voltage and current channels means that the individual accuracies of the resistors and capacitors in the circuit are not required to be known since the overall response is measured directly and then compensated for.

1) Voltage channel: The voltage channel was characterised across a range of frequencies of interest (1 Hz to 4 kHz) using an Audio Precision APX525 network analyser, which applies a chirp voltage signal and measures the response. The loopback response of the wires connecting the circuit to the network analyser was also measured separately and removed.

Fig. 5 shows the measured loopback response of the wires (grey), and of the full voltage channel (A1 and A2, red, broken dashed), and of the net channel end-to-end response (black) with the loopback response removed. It was found that the loopback response of the cables was the same as the response of the instrumentation amplifier A1 (not shown separately in the figure) since this has unity gain and a very high gain-bandwidth product, although there is a small deviation in phase between 1 kHz and 4 kHz likely caused by loopback cable inductance. Stage A2 introduces significant gain (40 dB) and has largely uniform magnitude response from 5Hz to 1 kHz.

At low frequencies ($<$ 100 Hz) the net magnitude rolls off and the phase increases due to the high pass filter; at high frequencies ($>$ 1 kHz) the magnitude rolls off and the phase decreases due to the low pass filter formed around A2 which has a gain-bandwidth product of 400-500 kHz. With a gain of 100 the measured -3dB point was at f = 3.77 kHz. This forms an anti-aliaising filter, as the analog-to-digital converter samples at 20 kHz.

The overall combined response for the voltage measurement channel can be represented fairly accurately by the second order transfer function equation (13):

$$G_1(s) = \frac{1}{1+s\tau_v}\frac{K_v s R_v C_v}{1+sR_vC_v} \tag{13}$$

where τ_v is the high frequency -3dB point, R_v is the value of the high pass filter resistor, C_v the capacitor and K_v the gain of A2. The response according to this transfer function is also shown in Fig. 5 (green, dashed); a small phase deviation is noted below 2 Hz and between 400 Hz and 3 kHz. For greatest accuracy the measured response data could be used instead of the fitted transfer function.

2) Current channel: The current channel uses a 1% precision 0.1 Ω shunt resistor (RS 363-6810) to produce a voltage drop proportional to the current. This is buffered by a differential amplifier, high pass filter and gain stage with the same design as A1 and A2 as already discussed for the voltage channel. The shunt resistor temperature coefficient of resistance is -50 to $+100$ ppm per °C [21]; therefore a large temperature change of 100 °C would be required to cause a resistance change of 1%. In our prototype system the resistor dissipates small amounts of power (up to 25 mW) and this does not cause appreciable temperature change. In a vehicle application, the temperature stability of the current measurement sensor would need to be considered in a similar way to ensure that an accurate measurement is made. Alternative sensors such as current transducers may be used; these have appreciable inductance and the calibration techniques outlined in this paper would need to be used to compensate for this.

Ideally, the current channel would have been calibrated by applying a known current signal and measuring the voltage response after A2. However, bench test equipment cannot drive very low impedances. Therefore the shunt resistor impedance was measured directly and this was combined with the characterisation of A1 and A2 in the same way as described for the voltage channel.

The shunt resistor behaves as a resistance in series with a small inductance and therefore has impedance given by:

$$Z_s = R_s + sL_s \tag{14}$$

where Z_s is the shunt resistor total impedance, R_s the resistance of the shunt and L_s the inductance, all in the frequency domain.

Using precision impedance measurement equipment (Bio-Logic VSP) it was found that R_s was very close to 0.1 Ω but that a small inductance (μH) was also present. Since

$$\angle Z_s = \tan^{-1}\left(\frac{\omega L_s}{R_s}\right) \tag{15}$$

therefore L_s can be calculated from the phase response of the shunt resistor. In most other applications this small inductance can be ignored, but for battery cells as we have demonstrated for the first time in this work it cannot be ignored since it distorts the measured battery impedance at frequencies above a few hundred Hz.

Therefore the response of the current measurement channel may be expressed using the transfer function:

$$G_2(s) = \frac{1}{1+s\tau_i}\frac{K_i s R_i C_i}{1+sR_iC_i}\left(R_s + sL_s\right) \tag{16}$$

where for the current channel τ_i is the high frequency -3dB point, R_i is the high pass filter resistor, C_i the capacitor and K_i the gain of A2.

In summary the measured calibration parameters for the experimental system are given in Table I.

TABLE I
CALIBRATION PARAMETERS FOR EXPERIMENTAL SYSTEM

τ_v	2.37e4 rad/s	K_v	101.4
R_v	9.95 kΩ	C_v	15.77 μF
τ_i	2.37e4 rad/s	K_i	101.4
R_i	9.95 kΩ	C_i	15.79 μF
L_s	4.2 μH	R_s	0.1 Ω

In order to apply the corrections to the estimated impedance $\hat{Z}(\omega)$ obtained with equation 7 so as to find the calibrated impedance $\hat{Z}_{cal}(\omega)$, $\hat{Z}(\omega)$ is multiplied by $G_2(s)/G_1(s)$ with $s = j\omega$, at each frequency of interest:

$$\hat{Z}_{cal}(\omega) = \hat{Z}(\omega)\frac{\frac{1}{1+s\tau_i}\frac{K_i s R_i C_i}{1+sR_iC_i}\left(R_s+sL_s\right)}{\frac{1}{1+s\tau_v}\frac{K_v s R_v C_v}{1+sR_vC_v}} \tag{17}$$

This calibrated impedance value may then be used for estimation of parameters such as SOC as described in section VI.

IV. RESULTS AND DISCUSSION USING ELECTRONIC LOAD

Using the TTi LD300 electronic load in current control mode, the impedance response of an A123 Systems LFP cell was measured using both a multisine excitation and broadband white noise excitation at ambient temperature conditions (between 18-21°C). The specifications of the cell are given in Table II. Due to the uni-directional nature of current flow into the load, a constant DC offset condition was imposed on the cell. Therefore test measurements were undertaken with $I_{DC} = 150$ mA and a superimposed peak-to-peak perturbation $I_{AC} = \pm 130$ mA. An example applied current perturbation from the electronic load and measured voltage response is shown in Fig. 6 where the waveform is comprised of 80 sinusoidal frequencies logarithmically spaced from 1 Hz to

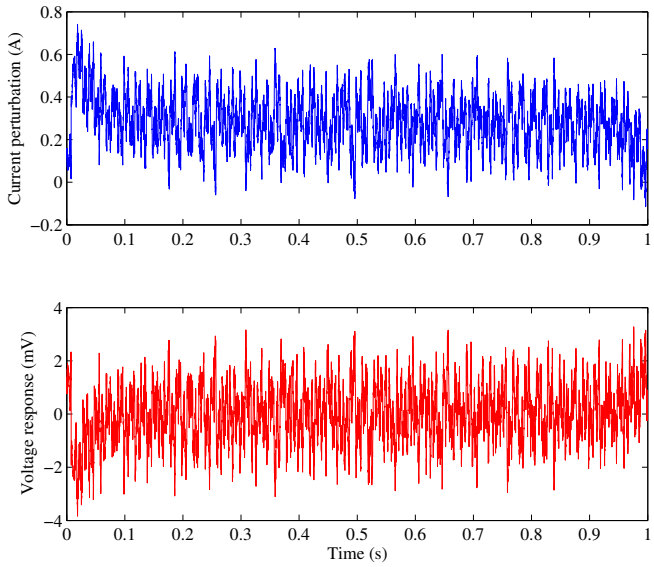

Fig. 6. Measured current and voltage, single cell with multi-sine excitation

2000 Hz. The bode plot comparison from 0.1 Hz to 2 kHz with multi-sine excitation is given in Fig. 7, which also compares data obtained using a motor controller as excitation source (see next section). In this figure the approaches outlined in this paper are compared with a high precision impedance measurement taken with a Bio-Logic VSP potentiostat system using the single frequency sweep method and the same DC offset and peak-to-peak test conditions. Fig. 8 shows the same comparison, but using broadband white noise as the excitation source instead. A summary of the uncertainty analysis for the electronic load data is given in Table III. The RMS uncertainty in magnitude is given by:

$$\epsilon_{RMS} = \sqrt{\frac{1}{N}\sum_{k=1}^{N}\left[|Z_1(\omega_k)| - |Z_2(\omega_k)|\right]^2} \tag{18}$$

where the subscript 1 indicates data from our system and the subscript 2 indicates data from the VSP potentiostat. Similarly the RMS uncertainty in phase is given by:

$$\angle\epsilon_{RMS} = \sqrt{\frac{1}{N}\sum_{k=1}^{N}\left[\angle Z_1(\omega_k) - \angle Z_2(\omega_k)\right]^2} \tag{19}$$

The percentage RMS uncertainty is calculated by dividing each absolute uncertainty by $|Z_2|$ before taking root mean square. These uncertainties are rather crude estimates of the fit between the data sets, tending for example to penalise outliers heavily, but they indicate the accuracy of our approach.

TABLE II
TEST CELL INFORMATION, [21]

Type	A123 Systems ANR26650
Dimensions (mm)	ϕ26 x 65
Nominal capacity (Ah)	2.3
Nominal voltage (V)	3.3

The comparison between multi-sine electronic load measurements and the Bio-Logic VSP, Fig. 7, is good across the

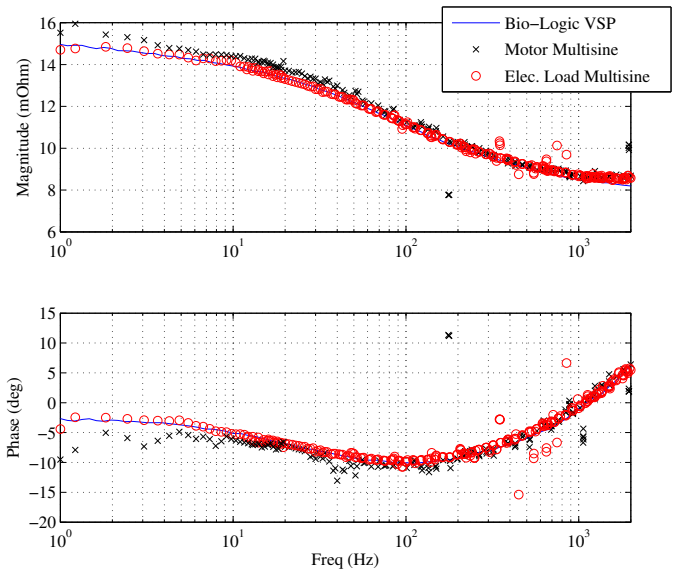

Fig. 7. Measured impedance comparison using multi-sine excitation

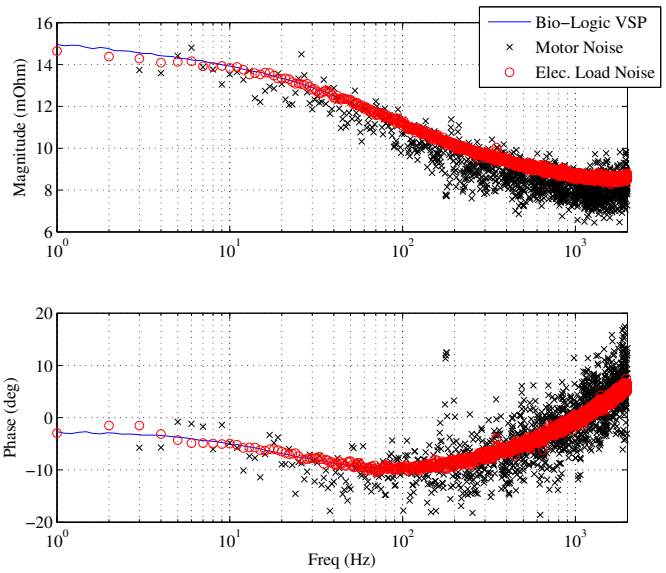

Fig. 8. Measured impedance comparison using broadband noise excitation

TABLE III
UNCERTAINTY ANALYSIS, ELECTRONIC LOAD DATA

Data set	ϵ_{RMS} (mΩ)	ϵ_{RMS} (%)	$\angle\epsilon_{RMS}$ (°)
Multi-sine	0.23	2.6	1.2
Multi-sine without 50N Hz outliers	0.16	1.9	0.6
Noise	0.22	2.6	0.7

full range of frequencies investigated (1 Hz to 2 kHz) with RMS uncertainties of less than 3% in magnitude and less than 1.5° RMS phase uncertainty, Table III. The multi-sine measurements exhibit outliers at odd harmonics of 50 Hz (the frequency of UK mains electricity). At these frequencies there is a strong coherence ($\gamma^2 > t_h$) between current and voltage (equation 12), but this is not caused by the battery impedance response, it is caused by narrowband external interference to both the voltage and current measurements. The use of multi-sine excitation concentrates the energy in the excitation signal into a number of discrete frequencies, whereas broadband noise excitation spreads the energy across a wide range of frequencies. Therefore the multi-sine results show increased sensitivity to narrowband interference, in this case from mains electricity. Removing these outliers slightly improves the RMS uncertainty (Table III).

The comparison between electronic load broadband noise measurements and Bio-Logic VSP, Fig. 8 is also very good, exhibiting similar RMS uncertainties to the multisine case but with lower absolute phase uncertainty, demonstrating that this approach is less sensitive to narrowband interference.

V. RESULTS AND DISCUSSION USING MOTOR CONTROLLER

To explore the use of a vehicle motor controller as a variable current source and sink connected to excite a battery pack, a small test rig, illustrated in Fig. 9, was built comprising a 30 W DC brushless servo motor (Maxon EC 45) with

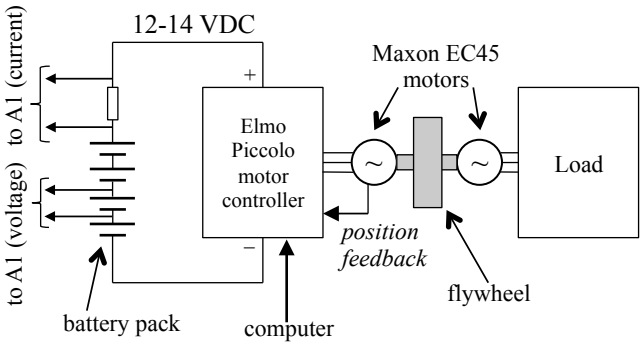

Fig. 9. Motor controller battery test system with 4 cells. Only one battery voltage measurement plus the current shunt is shown.

motor controller (Elmo Piccolo), directly coupled to a second 30 W electrical machine (also Maxon EC 45) which was connected to the electronic load, used to apply a DC load to the second electrical machine. The rig was powered by four A123 Systems LFP cells connected in series to form a 12-14 V DC supply. A steel flywheel with inertia approximately 0.15 g/m^2 was attached to the motor shafts to add mechanical energy storage and smooth speed fluctuations. The current fluctuations required to excite the battery result in torque fluctuations in the electrical machine, which result in small speed and position fluctuations. These are dampened by the flywheel as they would also be in a real vehicle application by the rotational inertia. The current fluctuations must be kept small in order to avoid significant torque ripple or problematic position errors. In our system, which used hall sensors for position feedback, there were no problems with position errors or loss of control. In a real application there will be a trade-off between the maximum acceptable current fluctuation and the amount of averaging required to achieve a good signal-to-noise ratio.

Since our primary interest is the use of the motor controller to

impose current fluctuations on the battery pack, it is important to consider the closed loop control bandwidth of the motor controller and the inductance of the motor coupled with the maximum bus voltage, as these both limit the rate of change of battery current. In this case the Elmo Piccolo motor controller has a maximum bandwidth of 3.2 kHz, so this is acceptable. The maximum rate of change of current is limited by the motor inductance and bus voltage:

$$\frac{dI}{dt} = \frac{V}{L} \tag{20}$$

where L = 0.56 mH for the motor used, $V \approx 12$ V, therefore maximum $dI/dt \approx 21429$ A/s. For a likely peak-to-peak current fluctuation of less than 500 mA this gives a minimum half cycle rise time of 23 μs i.e. a maximum frequency of around 21 kHz, which is also acceptable.

Using the motor test rig, both multi-sine and broadband noise excitation approaches were tested, and the results are shown in Figs. 7 and 8. A summary of uncertainty analysis data using the motor rig is given in Table IV using equations 18 and 19 to calculate the uncertainties.

TABLE IV
UNCERTAINTY ANALYSIS, MOTOR RIG DATA

Data set	ϵ_{RMS} (mΩ)	ϵ_{RMS} (%)	$\angle\epsilon_{RMS}$ ($^\circ$)
Multi-sine	0.55	5.8	3.4
Multi-sine, without outliers	0.26	2.5	1.4
Noise	0.20	2.2	2.7

In general the RMS impedance magnitude uncertainties using the motor rig are similar but slightly larger than those using the electronic load particularly in the case of the multi-sine excitation, where there is narrowband interference caused by the motor commutation. With noise excitation the magnitude uncertainties are very similar and slightly better than using the electronic load. With both multi-sine and noise however, the motor rig shows greater phase uncertainty than the electronic load. Below 10 Hz there is a deviation in both magnitude and phase caused by greater measurement noise and less averaging at these lower frequencies. Nonetheless these results show that in principle a motor controller and very low cost measurement circuit could be used to excite a battery with broadband noise to measure its impedance magnitude with an RMS systematic uncertainty within 3% and RMS systematic phase uncertainty within 3° compared to an expensive precision laboratory tester.

VI. TOWARDS ON-LINE SOC ESTIMATION

This paper has demonstrated that accurate impedance measurement may be carried out using an excitation current generated by a motor controller combined with a simple calibrated measurement circuit. Nonetheless the eventual aim is to estimate SOC from impedance in order to supplement or replace other SOC estimation techniques such as coulomb counting. Other metrics such as SOH may also be estimated but we concentrate first on SOC. Initially the impedance-based technique would be used during quiescent periods for example as part of a vehicle start-up process. This is to avoid large DC offset currents which change the battery equilibrium state with unknown consequences [20]. As more research is undertaken on the impact of DC current on impedance response, our system could also be used under heavy loading.

In larger battery packs for electric vehicles, individual cell voltage monitoring is typically undertaken for safety reasons. The method described here may therefore be applied to individual series connected cells. With parallel connected cells, voltage measurements for each individual cell cannot be decoupled and therefore only the average impedance of a parallel set may be measured.

The approach described here using an electrical machine as the excitation system represents a scaled-down prototype of a brushless DC drive system. This is relevant as a demonstrator because of the relationship in the scaling of the relevant parameters as the drive system is increased in power: in a full size electric vehicle, the battery packs will be larger, but so will the drive currents, and the perturbation current can be larger in absolute terms as the fraction of perturbation current to battery capacity can remain the same. For example in our prototype, a peak-to-peak perturbation current of 150 mA on a 2.3 Ah capacity cell represents a C-rate of 0.07 C (where 1 C is the current required to fully discharge a cell in one hour). In a real vehicle for example with battery pack capacity 24 kWh and voltage 300 V, a perturbation current of 5.4 A peak would achieve approximately a 0.07 C-rate.

Small signal equivalent circuit parameters such as series resistance R_0 or double layer capacitance, usually represented using constant phase elements (CPEs), may be fitted to measured impedance using an optimisation algorithm such as complex nonlinear least squares. A series of laboratory measurements relating parameters (extracted from impedance) to SOC and SOH must be taken beforehand. These would then be used in embedded hardware to estimate SOC and SOH from impedance. In order to investigate this approach, we have taken a series of measurements at various SOC and fitted parameters according to the equivalent circuit shown in Fig. 10 which includes two processes. The characteristic time constant of process 1 in the equivalent circuit is approximately 0.6 ms, and this process is related to lithium transport through the SEI, whereas process 2 with characteristic time constant approximately 2 ms is related to charge transfer at the anode and cathode [22]. In this circuit CPEs are used rather than conventional capacitors since the former provide a better fit with real electrochemical devices which have a distributed range of dynamics rather than a fixed time constant. The CPE is defined as $Z_{CPE} = 1/T\,(j\omega)^n$; for the case $n = 1$ this behaves as a conventional capacitor. From this data, the parameter showing the greatest variation with SOC for the A123 Systems LFP cells is the CPE parameter T_1 which shows a 2:1 variation across the range of SOCs, Fig. 11. In contrast other parameters such as the high frequency series resistance R_0 vary only by around 10% or less over the range of SOCs. However, in practice for LFP cells a combination of more

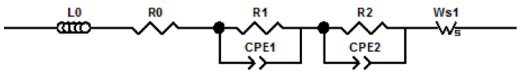

Fig. 10. LFP battery equivalent circuit

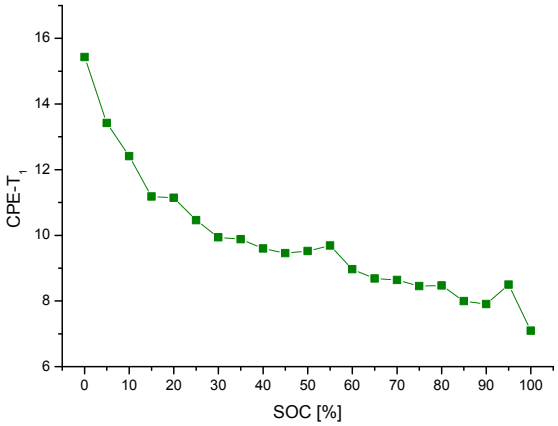

Fig. 11. Constant phase element CPE1 variation of admittance T_1 with SOC

than one parameter would need to be used for SOC estimation because the relationship between the parameters and SOC is not monotonic for this chemistry.

For other lithium-ion chemistries such as nickel-manganese-cobalt oxide (NMC), there is a clear monotonic parameter variation with SOC, as shown in Fig. 12 which shows the impedance variation with SOC for a Kokam 4.8 Ah prismatic NMC cell (SLPB 11043140H) at various SOC and ambient temperature, and Fig. 13 which shows the variation in R_1 and R_2, the resistances related to the SEI and charge transfer processes respectively as explained above. These were fitted to the impedance data using the same equivalent circuit model as the LFP cell.

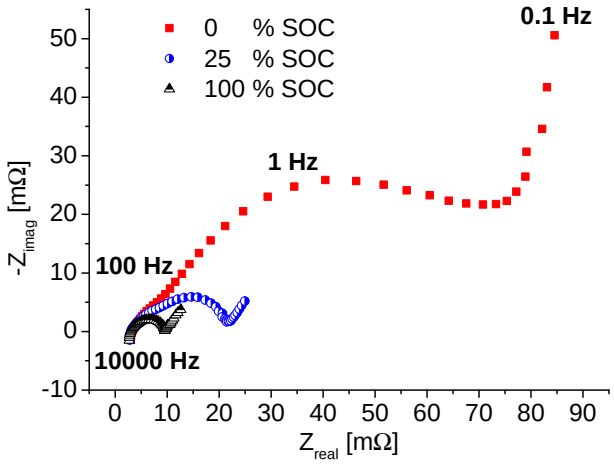

Fig. 12. NMC cell impedance variation with SOC

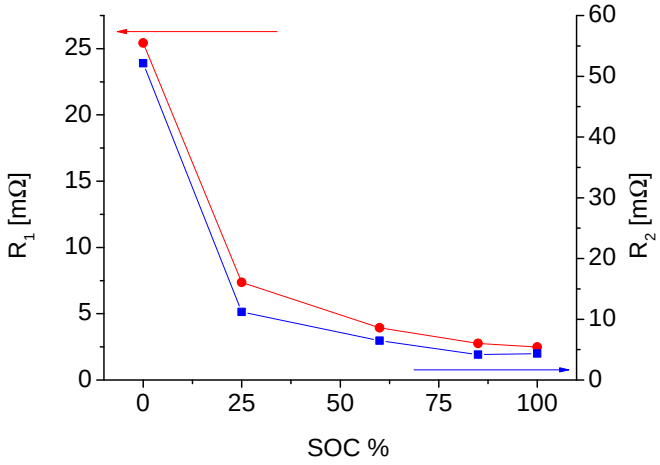

Fig. 13. SEI resistance R_1 and charge transfer resistance R_2 variation with SOC for NMC cell

VII. Conclusions

The present work has demonstrated a cost-effective battery impedance measurement system that could be used on-line in an application to measure impedance accurately at a range of frequencies of interest using the existing power electronics as the excitation source. A number of conclusions may be drawn:

The first is the importance of accounting for unwanted noise in the signal processing, and the coherence spectrum was used to estimate such noise in order to ignore poor quality data. On the other hand, broadband noise can in fact be used as a suitable excitation signal to measure impedance, and it may be possible therefore to measure impedance using noise already present in an application. Broadband noise excitation also has the advantage of being relatively immune to narrowband interference.

A second conclusion is the importance of accurate calibration of the voltage and current measurement channels in order to amplify the signals and remove any distorting effects from the measurement circuits. A straightforward procedure was demonstrated to characterise the measurement channels and fit their frequency responses with appropriate transfer functions. The effect of current shunt resistor inductance is noteworthy and this inductance must be measured and compensated for.

Lowest RMS uncertainties between measured impedance magnitudes and laboratory benchmark equipment were achieved using multi-sine perturbation pre-processed to remove narrowband outliers due to mains frequency interference and motor commutation. However both multi-sine and broadband noise signals could be used for impedance measurement together with a suitable parameter estimation optimisation algorithm.

Finally we discussed the implementation challenges of SOC estimation from impedance in both LFP and NMC cells, concluding that for the former SOC estimation would be challenging and a combination of fitted parameters would need

to be used, whereas for the latter there are clear monotonically varying parameters from which SOC may be estimated.

VIII. Acknowledgements

This work was funded by the UK Engineering and Physical Sciences Research Council Grant No. EP/H05037X/1. We are also very grateful for the assistance of Billy Wu at Imperial College who recorded the EIS data for the NMC cell.

References

[1] E. Meissner and G. Richter, "Battery Monitoring and Electrical Energy Management: Precondition for future vehicle electric power systems," *Journal of Power Sources*, vol. 116, no. 1-2, pp. 79–98, 2003.

[2] G. Plett, "Extended Kalman filtering for battery management systems of LiPB-based HEV battery packs, Part 1: Background," *Journal of Power Sources*, vol. 134, no. 2, pp. 252–261, 2004.

[3] D. V. Do, C. Forgez, K. El Kadri Benkara, and G. Friedrich, "Impedance Observer for a Li-Ion Battery Using Kalman Filter," *IEEE Transactions on Vehicular Technology*, vol. 58, no. 8, pp. 3930–3937, 2009. [Online]. Available: http://ieeexplore.ieee.org/lpdocs/epic03/wrapper.htm?arnumber=5184857

[4] U. Troltzsch, O. Kanoun, and H. Trankler, "Characterizing aging effects of lithium ion batteries by impedance spectroscopy," *Electrochimica Acta*, vol. 51, no. 8-9, pp. 1664–1672, 2006.

[5] G. J. Offer, V. Yufit, D. A. Howey, B. Wu, and N. P. Brandon, "Module design and fault diagnosis in electric vehicle batteries," *Journal of Power Sources*, vol. 206, pp. 383–392, 2012. [Online]. Available: http://linkinghub.elsevier.com/retrieve/pii/S0378775312001863

[6] L. Lu, X. Han, J. Li, J. Hua, M. Ouyang, and Y. Zheng, "A review on the key issues for lithium-ion battery management in electric vehicles," *Journal of Power Sources*, vol. 226, pp. 272–288, 2013.

[7] R. Robinson, "System noise as a signal source for impedance measurements on batteries connected to operating equipment," *Journal of Power Sources*, vol. 42, no. 3, pp. 381–388, 1993.

[8] O. Bohlen, S. Buller, R. De Doncker, M. Gelbke, and R. Naumann, "Impedance based battery diagnosis for automotive applications," *IEEE 35th Annual Power Electronics Specialists Conference*, pp. 2792–2797, 2004.

[9] H. Blanke, O. Bohlen, S. Buller, R. Dedoncker, B. Fricke, A. Hammouche, D. Linzen, M. Thele, and D. Sauer, "Impedance measurements on lead acid batteries for state-of-charge, state-of-health and cranking capability prognosis in electric and hybrid electric vehicles," *Journal of Power Sources*, vol. 144, no. 2, pp. 418–425, 2005.

[10] J. P. Christophersen, C. G. Motloch, J. L. Morrison, I. B. Donnellan, and W. H. Morrison, "Impedance Noise Identification for State-of- Health Prognostics," *43rd Power Sources Conference*, 2008.

[11] J. Morrison, W. Morrison, and J. Christophersen, "Method of detecting system function by measuring frequency response," US Patent 20 100 274 510, 2010.

[12] M. Doyle, J. P. Meyers, and J. Newman, "Computer Simulations of the Impedance Response of Lithium Rechargeable Batteries," *Journal of The Electrochemical Society*, vol. 147, no. 1, p. 99, 2000.

[13] E. Barsoukov, J. H. Kim, D. H. Kim, K. S. Hwang, C. O. Yoon, and H. Lee, "Parametric analysis using impedance spectroscopy: relationship between material properties and battery performance," *Journal of New Materials for Electrochemical Systems*, vol. 3, pp. 303–310, 2000.

[14] J. Remmlinger, M. Buchholz, M. Meiler, P. Bernreuter, and K. Dietmayer, "State-of-health monitoring of lithium-ion batteries in electric vehicles by on-board internal resistance estimation," *Journal of Power Sources*, vol. 196, no. 12, pp. 5357–5363, 2011.

[15] M. A. Roscher, J. Assfalg, and O. S. Bohlen, "Detection of Utilizable Capacity Deterioration in Battery Systems," *IEEE Transactions on Vehicular Technology*, vol. 60, no. 1, pp. 98–103, 2011. [Online]. Available: http://ieeexplore.ieee.org/lpdocs/epic03/wrapper.htm?arnumber=5613947

[16] L. Ljung, *System Identification: Theory for the User*, 2nd ed. Prentice Hall, 1999.

[17] A. Fairweather, M. Foster, and D. Stone, "VRLA battery parameter identification using pseudo random binary sequences (PRBS)," *5th IET International Conference on Power Electronics, Machines and Drives (PEMD 2010)*, pp. TU244–TU244, 2010.

[18] J. Schwarzenbach and K. Gill, *System modelling and control*, 3rd ed. Edward Arnold, 1991.

[19] A. Jossen, "Fundamentals of battery dynamics," *Journal of Power Sources*, vol. 154, no. 2, pp. 530–538, 2006. [Online]. Available: http://linkinghub.elsevier.com/retrieve/pii/S0378775305014321

[20] W. Waag, S. Käbitz, and D. U. Sauer, "Experimental investigation of the lithium-ion battery impedance characteristic at various conditions and aging states and its influence on the application," *Applied Energy*, vol. 102, pp. 885–897, 2012. [Online]. Available: http://linkinghub.elsevier.com/retrieve/pii/S030626191200671X

[21] A123, "Nanophosphate High Power Lithium Ion Cell ANR26650M1-B Data Sheet," 2011. [Online]. Available: http://info.a123systems.com/data-sheet-26650-cylindrical-cell/

[22] T. K. Dong, A. Kirchev, F. Mattera, and Y. Bultel, "Modeling of Lithium Iron Phosphate Batteries by an Equivalent Electrical Circuit: Method of Model Parameterization and Simulation," *ECS Transactions*, vol. 25, no. 35, pp. 131–138, 2010. [Online]. Available: http://ecst.ecsdl.org/cgi/doi/10.1149/1.3414011

David A. Howey (M 10), PhD (Imperial 2010) MA MEng (Cantab. 2002), is a Lecturer in the Energy and Power Group at the Department of Engineering Science, University of Oxford. His research interests are condition monitoring and management of electric vehicle components. He leads projects on fast electrochemical modelling, model-based battery management systems, battery thermal management, and motor degradation.

Paul D. Mitcheson (M 02, SM 12) MEng (Imperial 2001) PhD (Imperial 2005) is currently a Senior Lecturer with the Control and Power Research Group, Department of Electrical and Electronic Engineering, Imperial College London. His research interests are in power electronics across various scales from energy harvesting to HVDC and includes interfaces for inductive power transfer. He has a parallel stream of work on in-situ battery status monitoring.

Vladimir Yufit is a Postdoctoral Research Associate in the Department of Earth Science and Engineering at Imperial College London. He obtained his PhD from Tel Aviv University (Israel) leading pioneering work on development of three-dimensional thin film lithium-ion microbatteries. His research interests include rechargeable non-aqueous batteries; PEM, alkaline and solid oxide fuel cells; redox flow batteries and regenerative fuel cells; supercapacitors and advanced characterisation techniques.

Gregory Offer is a Lecturer in Mechanical Engineering and holds an EPSRC Career Acceleration Fellowship at Imperial College London. He is an electrochemist working at the interface between the fundamental science and systems engineering of fuel cells, batteries and supercapacitors. His research interests focus on understanding the degradation and failure of such components in automotive applications and the impact on system design and vice versa.

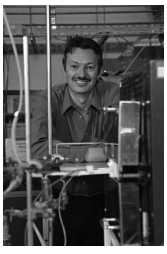

Prof Nigel P. Brandon OBE FREng is Director of the Energy Futures Lab at Imperial College London. His research interests focus on the science and engineering of electrochemical power sources, with a particular focus on batteries and fuel cells.